https://doi.org/10.5194/egusphere-2022-142
Preprint. Discussion started: 28 April 2022

Modelling the impact of anthropogenic measures on saltwater intrusion in the Weser estuary

Pia Kolb[1], Anna Zorndt[1], Hans Burchard[2], Ulf Gräwe[2], and Frank Kösters[1]

[1]Federal Waterways Engineering and Research Institute, Wedeler Landstraße 157, 22559 Hamburg, Germany
[2]Leibniz Institute for Baltic Sea Research Warnemünde, Seestraße 15, 18119 Rostock, Germany

Correspondence to: Pia Kolb (pia.kolb@baw.de)

Abstract. The Weser estuary has been subject to profound changes in topography in the last hundred years through natural variations and river engineering measures, leading to strong changes in hydrodynamics. These changes are also expected to have affected the dynamics of saltwater intrusion. Using numerical modelling, we examined saltwater intrusion in the Weser estuary in four different system states (1966, 1972, 1981, 2012). Models of each system state were set up with the respective topography and boundary values. The resolution of historical and recent topographical data is usually not comparable, which needs to be compensated, e.g., by calibration of roughness parameters. Therefore, each model was individually calibrated and validated. In simulations of one hydrological year for each system state (hindcasting study), the influence of topography is overshadowed by the effects of other factors, particularly river discharge. At times of identical discharge, results indicate a landward shift of the salinity front between 1966 and 2012. Subsequent simulations with different topographies but identical boundary conditions (scenario study) confirm that topographic changes in the Weser estuary affected saltwater intrusion. Solely through the topography changes, at a discharge of 300 $m^3 s^{-1}$, the position of the tidally averaged and depth-averaged salinity front shifted landwards by about 2.5 km between 1972 and 1981 due to deepening measures in the Lower Weser between these years. It shifted by another 1 km between 1981 and 2012. These changes are significant but comparatively small, since due to seasonal variations in run-off, the tidally averaged salinity intrusion can vary by more than 20 km.

Short summary:

River engineering measures strongly changed tidal dynamics in the Weser estuary. We studied the effect on saltwater intrusion with numerical models. Our analysis shows that a deepening of the navigation channel causes saltwater to intrude further into the Weser estuary. This effect is mostly outweighed by the natural variability of river discharge. In the study, it proved essential to recalibrate individual hindcast models due to different resolutions of underlying bathymetrical data.

Keywords: Estuaries, numerical models, shelf seas, seabed morphology, Weser estuary, estuary deepening, morphological changes, saltwater intrusion

https://doi.org/10.5194/egusphere-2022-142
Preprint. Discussion started: 28 April 2022

1 Introduction

Estuaries are ever-changing systems. Natural processes and anthropogenic interventions determine the topography and conditions we observe in estuaries today. Due to the high economic importance of estuaries as shipping routes, further interventions to consolidate navigation channels can be expected. In order to manage adverse effects, predictability of changes associated with the engineering measures is essential. As a response to deepening measures, significant changes in hydrodynamics have been observed in estuaries. When water depth increases, the effect of bottom friction decreases. This reduces the dissipation of tidal energy, resulting in a larger tidal amplitude and often in phase shifts in the ebb and flood current durations and velocities (Winterwerp et al., 2013; Ralston et al., 2019). At the same time, changes in mixing processes can occur, possibly affecting the length of saltwater intrusion (Grasso and Le Hir, 2019). Saltwater intrusion is directly linked to water quality and sediment transport processes (Burchard et al., 2018a) and thus needs to be monitored.

The effect of topography changes on saltwater intrusion depends on the physical mechanisms that control salt transport in estuaries. Most important are the net advection, driven by freshwater discharge, and the estuarine circulation, i.e. the tidally averaged estuarine exchange flow. One driver of the estuarine circulation is the combination of the seaward barotropic (depth-independent) and the landward baroclinic (increasing with depth) pressure gradient, which results in a seaward flow of estuarine water near the surface and landward flow of dense water near the bed. This is known as the gravitational circulation (Geyer and MacCready, 2014). Depending on the estuary´s geometry and tidal forcing, strain-induced periodic stratification (SIPS) can occur with stratification during ebb and mixing during flood (Simpson et al., 1990). This tidal asymmetry enhances estuarine circulation (Jay and Musiak, 1994) and has been referred to as tidal straining circulation (Burchard et al., 2011; Geyer and MacCready, 2014) or eddy viscosity – shear covariance (ESCO, Dijkstra et al., 2017). Other drivers include e.g. lateral momentum advection (Burchard et al., 2011) or estuarine convergence (Ianniello, 1979; Burchard et al., 2014). The strength of salt transport mechanisms depends on the water depth and it is therefore expected that channel deepening affects saltwater intrusion (Andrews et al., 2017).

Studies have been conducted in estuaries worldwide to try to quantify the impact of changes in topography, i.e., channel deepening or widening, on saltwater intrusion. In recent studies, numerical models with different topographies have been used to examine mixing and transport processes in estuaries before and after implementing engineering measures. Among others, such investigations have been conducted for the San Francisco estuary, US (Andrews et al., 2017), the Hudson River estuary, US (Ralston and Geyer, 2019), the Danshui River estuary system, Taiwan (Liu et al., 2020), the Seine estuary, France (Grasso and Le Hir, 2019), and the Ems estuary, Germany (van Maren et al., 2015).

Generally, it was found that a deepening of the river channel is associated with a landward shift of the brackish water zone. Several studies explain the increase in landward salt transport with an increase in the estuarine circulation and a decrease in vertical mixing processes, which occur due to the larger water depths (Grasso and Le Hir, 2019; Andrews et al., 2017; van Maren et al., 2015). In the case of the Danshui river estuary, some channels have been deeper in the predevelopment state, which goes along with increased gravitational circulation and a further upstream limit of the salinity intrusion in the

https://doi.org/10.5194/egusphere-2022-142
Preprint. Discussion started: 28 April 2022

predevelopment state (Liu et al., 2020). All the other above-mentioned estuaries are deeper in the present state. Grasso and Le Hir (2019) investigated key estuarine processes in the Seine estuary in 1960 and 2010 and detected a relative increase in gravitational circulation and stratification. This caused an up-estuary shift of the salinity front and changed the response of saltwater intrusion to tides and discharge. Ralston and Geyer (2019) examined the Hudson River estuary in the present state and the predevelopment state. They detect an increase in saltwater intrusion and stratification, but only a minor change in estuarine circulation and no change in the response of saltwater intrusion to river discharge. The authors conclude that dredging in the Hudson did not significantly change estuarine exchange processes.

In most of the abovementioned studies, a numerical model of the respective estuary in the present state was set up and calibrated. Different model topographies were subsequently inserted to represent earlier states of the estuary (Ralston and Geyer, 2019; Grasso and Le Hir, 2019; Liu et al., 2020). Models representing earlier system states of the estuary were not calibrated. However, differences in bed roughness are expected to occur between the system states due to sediment redistribution and changes in bed forms, which are usually not resolved in the models. Van Maren et al. (2015) calibrated models of the Ems estuary for different system states and obtained significantly larger roughness values with historical bathymetries compared to the present state. This is attributed to the observation that sediment in the Ems estuary has successively become finer in the last decades. The authors conclude that changes in bed roughness can strongly contribute to shifts in hydrodynamics and transport processes. In addition to shifts in bed roughness, the resolution of data which are used to generate model topographies may differ for the system states, with an effect on form drag. Thus, the system behaviour at different points of time with different topographies might be better represented with individually calibrated models.

In the Weser estuary, no model-based examinations have yet been conducted to examine the effect of anthropogenic measures on saltwater intrusion. Instead, saltwater intrusion and influencing parameters have been tracked by measurements and attempts have been made to separate the impact of different factors (Krause, 1979; Grabemann et al., 1983). However, many factors affect saltwater intrusion on different time scales and it has therefore not been possible to isolate the impact of topography variations (Grabemann et al., 1983). Within each tidal cycle, the position of the brackish water zone shifts by more than 15 km along the navigation channel of the Weser (Kösters et al., 2014). Changes in tidal components, meteorological conditions, long-term variations of the salinity of the North Sea, and variations in discharge also affect the position of the brackish water zone (Grabemann et al., 1983). Due to variations in discharge, the tidally averaged salinity intrusion shifts by more than 20 km, whereby the impact is larger for low-discharge conditions than high-discharge conditions (Kösters et al., 2014).

This study aims to systematically quantify saltwater intrusion in a real tidal estuary in different system states and to determine to what degree anthropogenic measures impact saltwater intrusion in the estuary. As an example, we studied the Weser estuary in the German Bight and set up numerical model simulations in four different system states (1966, 1972, 1981, 2012). In contrast to most previous studies, we individually calibrated each model and conducted simulations with realistic and with idealized forcing. In this paper, we describe the model setup and simulation results. We discuss the methodology, the

https://doi.org/10.5194/egusphere-2022-142
Preprint. Discussion started: 28 April 2022

importance of calibration for the model-based examination with different model topographies, and the effect of channel deepening on processes governing saltwater intrusion.

2 Study site: the Weser estuary

2.1 Geomorphology and hydrology

The Weser estuary, located in Northern Germany, is of high ecological and economic importance. It is divided into two sections: the Lower Weser and the Outer Weser (see Fig. 1). The Lower Weser stretches from the tidal weir at Bremen-Hemelingen (km 0, the tidal limit) to Bremerhaven (km 66.7). The funnel-shaped Outer Weser starts from Bremerhaven and opens towards the North Sea (km 126). The estuary is an important shipping channel, providing access to the container terminal of Bremerhaven, the port of Bremen, and several smaller ports. In 1941–2015, the mean annual discharge, measured at station Intschede, was 321 $m^3 s^{-1}$ with high seasonal variability (NLWKN, 2018). In the same period, the mean low discharge (mean value of the smallest discharge of each year 1941–2015) was 116 $m^3 s^{-1}$ and the mean high discharge (mean value of the largest discharge of each year 1941–2015) was 1200 $m^3 s^{-1}$ (NLWKN, 2018).

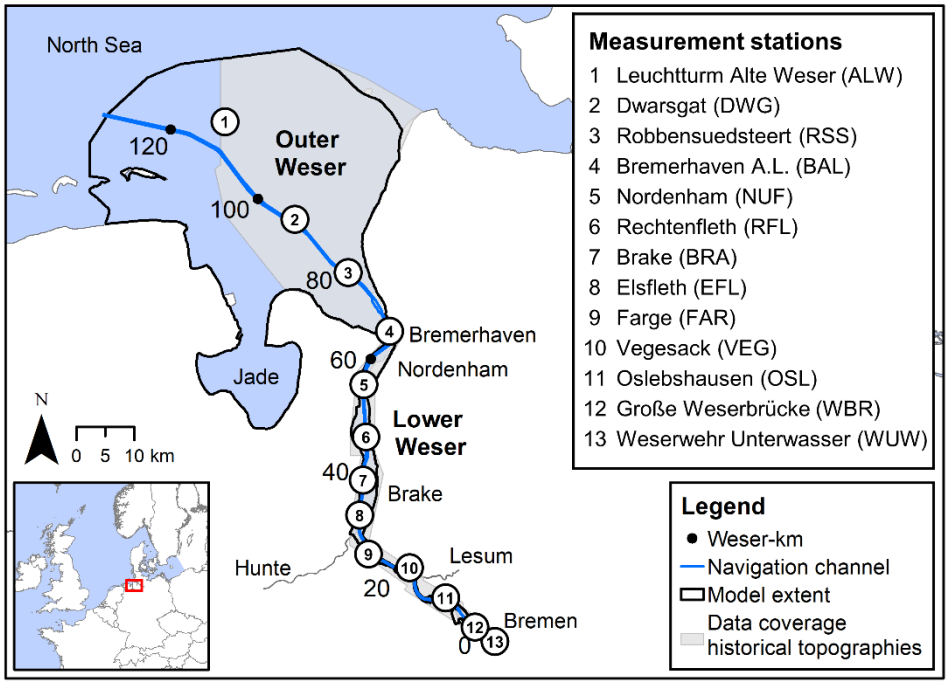

Figure 1. Map of the model area and distance along the navigation channel from the tidal weir at Bremen (Weser-km) with data coverage for historical topographies displayed in grey.

The semidiurnal tidal wave from the North Sea propagates through the Weser estuary in about three hours. At the northern part of the Outer Weser, the tidal range is 2.8 m. On its way through the estuary, it increases to 3.8 m near Bremerhaven due

https://doi.org/10.5194/egusphere-2022-142
Preprint. Discussion started: 28 April 2022

to estuarine convergence, slightly decreases between km 50 and km 30, and increases to 4.1 m near Bremen. In most stretches of the navigation channel of the Lower and Outer Weser, ebb currents are slightly stronger than flood currents. Flood currents dominate in some stretches, such as Weser-km 80–95 (Lange et al., 2008).

Before mixing with seawater, the river Weser has an initial salinity of about 0.5 psu as a caustic potash solution is discharged further upstream. The mean position of the 2 psu isohaline is located at Weser-km 45 at the reversal from flood to ebb (high water slack) and km 60 at the reversal from ebb to flood (low water slack) (Lange et al., 2008).

2.2 Historical development

The topography of the Weser estuary has been strongly altered through river deepening and correction measures since the end of the 19th century. The main objective of these measures was to establish and maintain a continuous shipping route with sufficient depth and width for ships of increasing size to pass through (Wetzel, 1988).

Since 1960, three major deepening measures have been conducted. The Outer Weser was modified in 1969–1971 to create a continuous depth of nautical chart datum 'Seekartennull' (SKN) -12 m and in 1998–1999 to increase the depth to SKN -14 m (Lange et al., 2008; Wetzel, 1988). Engineering measures at the Lower Weser were conducted in 1973–1978. Thereby, the stretch between Brake and Bremen was deepened to nautical chart datum SKN -9 m, and the stretch between Bremerhaven and Nordenham to SKN -11 m (Lange et al., 2008; Wetzel, 1988). Starting in 1982, additional groynes were constructed in the Lower Weser to regulate the flow further. The mouth of the Ochtum tributary was relocated in 1972–1976, and the mouth of the Hunte tributary in 1979. Moreover, regular dredging measures for maintenance were conducted in the navigation channel (Wetzel, 1988). The bathymetry height along the navigation channel in the four system states is depicted in Fig 2.

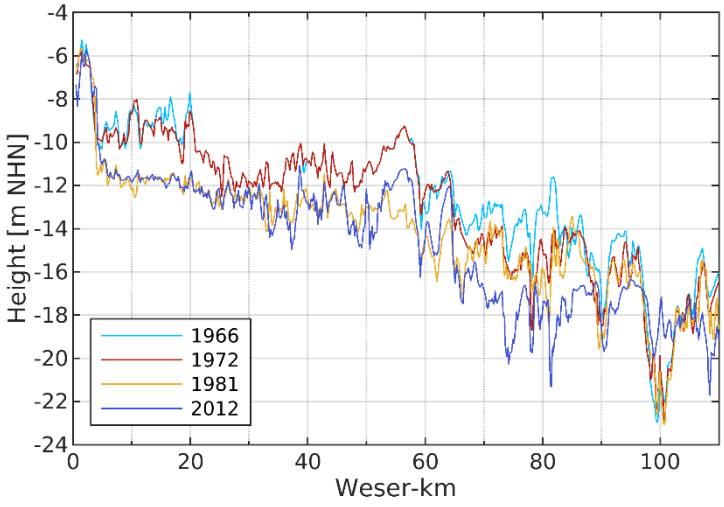

Figure 2. Height along the navigation channel (200-300 m width) in the Weser estuary in different years, based on model topographies.

https://doi.org/10.5194/egusphere-2022-142
Preprint. Discussion started: 28 April 2022

3 Methods

We built numerical models of the Weser estuary in four system states: 1966, 1972, 1981, and 2012. A simulation of one hydrological year was conducted for each model with realistic forcing to hindcast hydrodynamics and saltwater intrusion ('hindcast study'). Results from previous calibration runs with respective topographies were used as initial conditions and a spin-up time of four weeks was applied. Additionally, simulations of each system state, but with identical forcing, were conducted and analysed for one spring–neap cycle (after six weeks spin-up time) so that the impact of topography changes and roughness changes could be individually evaluated ('scenario study'). In all simulations, salinity along the navigation channel (see Fig. 1) was analysed and the location of the salinity front, which was defined as the vertically averaged 5 psu isohaline, was calculated.

3.1 Description of the numerical model

Numerical simulations are based on UnTRIM² (Casulli, 2008). UnTRIM² solves the Reynolds-averaged Navier Stokes equations, the continuity equation, and transport equations based on a semi-implicit finite volume / finite difference approach to calculate current velocities, surface elevations, and tracer concentrations (Casulli and Walters, 2000). The equations are solved on a horizontally unstructured grid with vertical z-layers of 1 m thickness. The model considers 3D hydrodynamics, daily freshwater discharge from the Weser, and the transport of salinity and heat. Vertical turbulent mixing was estimated with a two-equation k-ε model; horizontal mixing was modelled with a constant viscosity and diffusivity. UnTRIM² was coupled with the sediment transport model SediMorph (BAW, 2002) to calculate bottom roughness. For simplicity, we neglected sediment transport in this study. The model is well-suited to simulate flows in estuaries, as the algorithm accurately preserves mass where wetting and drying occurs (Casulli, 2008). For example, it has been used to simulate flows in San Francisco Bay (Andrews et al., 2017), the German Bight (Hagen et al., 2021a; Rasquin et al., 2020), and the Weser Estuary (Kösters et al., 2014).

3.2 Model topographies

The model area includes the Lower Weser, the Outer Weser, and the adjacent Jade (see Fig. 1). Tributaries of the Weser and their discharge are not represented, as topographical and hydrographic data of the tributaries are not available for all system states. The same unstructured orthogonal calculation grid was used in all models. It contains cells of different sizes, arranged to increase the resolution in areas of interest. Cell spacing in the navigation channel is 50–250 m.

Model topographies were created by interpolating respective topographical data on the calculation grid, smoothening transitions, and correcting essential landscape features. The model topography of 2012 is based on elevation data from multibeam echosounder measurements and laser scanning flights. Model topographies of the other system states are based on historical maps with diverse land and hydrographic surveying data. These maps have been compiled to historical topographies of the Lower and Outer Weser (see Fig. 1, grey area) in different historical system states (BAW, 2020, 2021). We interpolated

https://doi.org/10.5194/egusphere-2022-142
Preprint. Discussion started: 28 April 2022

the topographical data from 1966, 1972, and 1981 on the computational grid preserving the wet volume and filled the remaining area of the North Sea and Jade with bathymetrical data from 2012. Subsequently, we corrected important landmarks and structures such as summer dikes, side channels, constructions, and the transition between Outer Weser (historical topographic data) and Jade (topographic data of 2012) in the case of the model topographies 1966, 1972, and 1981.

Please note that temporal and spatial data coverage, which determines the models' quality and level of details, varies for the different decades. For the generation of the historical topographies, data were scarcer and less detailed than the present state. Therefore, the resolution of small-scale features such as bedforms in the different model topographies is not directly comparable. With less representation of small-scale features in historical topographies, the bathymetry is smoother and the roughness effect of varying topography represented in the grid is lower. This influences the model results. As an indicator for the resolution of the different model topographies, we evaluated the depth variation along the estuary in the different setups. We extracted depth values h_1 to h_n at n defined points along a transect along the navigation channel (every 50 m). Then, we calculated the average depth variation Δ_h between adjacent points with

$$\Delta_h = \frac{\sum_{i=1}^{n-1} |h_{i+1} - h_i|}{n-1}. \quad (1)$$

Our results show that between Bremen and Nordenham (Weser-km 55.8), the depth variation in the 2012 model is almost twice as high as in the historical systems states (see Table 1). This indicates a higher resolution of the original topographic data with a representation of small-scale features and a higher form drag. Minor differences in depth variation do also occur between the individual model topographies. To account for the different resolutions of the underlying bathymetric data and their effect on form drag, we individually calibrated the models of each system state with the respective topographies (see Section 3.4).

Table 1. Depth variation (see Eq. (1)) along a transect in different system states between Bremen and Nordenham (Weser-km 1.5–55.8) and between Nordenham and the North Sea (Weser-km 55.8–126).

	1966	1972	1981	2012
Along Weser-km 1.5-55.8 (in m)	0.15	0.15	0.16	0.29
Along Weser-km 55.8-126 (in m)	0.10	0.11	0.12	0.12

3.3 Initial sediment distribution

We prescribed an identical initial sediment distribution in all models based on diverse sediment samples as described in Milbradt et al. (2015). The sediment distribution represents the system state 2012; data from previous years were additionally used at locations with insufficient data coverage. The distribution comprises eight fractions of sediments: very coarse sand, coarse sand, medium sand, fine sand, very fine sand, coarse silt, medium silt, and fine silt. Even though it is very likely that

https://doi.org/10.5194/egusphere-2022-142
Preprint. Discussion started: 28 April 2022

the sediment distribution in the Weser estuary has changed between the system states 1966, 1972, 1981, and 2012, we decided to use the same initial sediment distribution in all models as historical data are scarce. We assume that the effect of this simplification is small. In the models, the initial sediment distribution is used for roughness calculation based on sediment type and bedform prediction (see Section 3.6).

3.4 Model forcing

As boundary conditions, we prescribed time series for salinity, temperature, and water level at the seaward boundary to the North Sea. Furthermore, we provided salinity, temperature, and discharge of the Weser at the landward boundary. The hindcast study aimed to represent the system states as realistically as possible. Measurement values were retrieved from the Waterways and Shipping Authorities Bremerhaven, Bremen and Hann.-Münden and time series were constructed by linear interpolation between observations. Measured values were available for most parameters, but not for water level and salinity at the seaward model boundary in the North Sea in 1966, 1972, and 1981. For the water level however, historical records for tidal high and low water levels were available for the station 'Leuchtturm Alte Weser' (ALW, see Fig. 1) close to the model boundary. Thus, we generated a synthetic time series of 1965–2012 by reconstructing the astronomical tide at station ALW, fitting the signal to measured high water and low water values and inducing a phase shift and amplitude amplification to account for the distance of the station to the model boundary. The synthetic time series was used for all models for the sake of consistency, even though measured records of water level at ALW would have been available for the hindcast model of 2012. Salinities at four positions along the open boundary were approximated utilising neural networks of two layers (55 and 11 neurons) with a Levenberg–Marquardt algorithm. For each position, 100 networks were trained with salinity values of 1996–2016, which were extracted from a validated model of the German bight, the Easy GSH model (Hagen et al., 2021b). As reference data, the tidal range and tidal mean water level at station ALW, salinity records at Helgoland station (Wiltshire et al., 2008), and the discharge of the Weser and Elbe were used. Subsequently, the correlation of network results and the extracted target salinity values were calculated and the best network for each position was selected. With the selected networks, salinity at each position was predicted for all system states (1965–2012). For the hindcast model 2012, consistent boundary values would have been available from measurements or from the aforementioned Easy GSH model. However, we stuck to the neural networks to ensure consistency between the models of different system states. Moreover, boundary values for salinity and temperature at the landward boundary for the hindcast model 1966 were reconstructed. For salinity, a relationship between discharge and salinity was derived based on measured data from 1967–1968, where the amount of potash discharging can be assumed to be similar to 1966. Salinity values for the hydrological year 1966 were calculated based on measured discharge values with

$$S_{river} = 6 * 10^{-7} \frac{psu}{m^6\, s^{-2}} * Q^2 - 0.0017 \frac{psu}{m^3\, s^{-1}} * Q + 2.0759\, psu, \quad (2)$$

https://doi.org/10.5194/egusphere-2022-142
Preprint. Discussion started: 28 April 2022

where S_{river} is salinity and Q is discharge. For temperature, measured values of 1968 were used instead of 1966, as the variations over the years were assumed to be similar and temperature is only of secondary importance in this study.

In contrast to the hindcast study, we used identical boundary values in all simulations for the scenario study. The synthetic time series of the hindcast model 2012 was used for water level at the open boundary. For all other parameters, cross-scenario boundary values were generated; representing an average of the four system states (see Table 2).

Table 2. Boundary values in hindcast study (realistic forcing) and scenario study (identical forcing). In each study, simulations of system state 1966, 1972, 1981, and 2012 were conducted. For the hindcast model of 1966, no measured values for salinity and temperature in the Weser were available. Therefore, salinity values were approximated based on the relationship to discharge (see Eq. (2)); temperature values were replaced with values of 1968, the closest year with available records.

Boundary condition	Hindcast study	Scenario study
North Sea water level	Synthetic time series (of respective year)	Synthetic time series (of 2012)
North Sea salinity	Time series generated with neural networks	28.7 psu
North Sea temperature	Time series constructed from observations	15.5 °C
Weser discharge	Time series constructed from observations	300 $m^3 s^{-1}$
Weser salinity	Time series constructed from observations	1.2 psu
Weser temperature	Time series constructed from observations	19.9 °C

3.5 Analysis methods

Model results were analysed by evaluation of tidal characteristic values, which describe the tidal curve and facilitate characterization of the system's behaviour and comparison between simulations (Lang, 2003). Thus, for example, the tidal range and the minimum, mean, and maximum salinity per tidal cycle were calculated in each scenario and compared.

In addition, the position of the brackish water zone was calculated for all model results by determining the position of the vertically averaged 5 psu and 20 psu isohaline along the navigation channel (see Fig. 1) based on the mean salinity per tidal cycle. The saltwater intrusion length was defined as the distance from the estuary mouth (Weser-km 126.2, see Fig. 1) to the mean 5 psu isohaline along the navigation channel. Further, the potential energy anomaly Φ was evaluated. According to Simpson (1981), the potential energy anomaly is the energy required to homogenise the water column with given density stratification instantaneously. Burchard and Hofmeister (2008) define it as

$$\Phi = \frac{1}{D}\int_{-H}^{\eta} gz(\bar{\rho}-\rho)\,dz;\ \bar{\rho} = \frac{1}{D}\int_{-H}^{\eta}\rho\,dz\,, \tag{3}$$

where H is the mean water depth, η is the water level elevation, $D = \eta+H$ is the actual water depth, g is the gravitational acceleration, and ρ is the density. Thus, an increase in potential energy anomaly indicates an increase in stratification.

https://doi.org/10.5194/egusphere-2022-142
Preprint. Discussion started: 28 April 2022

3.6 Calibration and validation

Models of each system state were calibrated in two steps by adjustment of the roughness settings: first, tuning of a form roughness predictor, and second, definition of an additional roughness in the Lower Weser. Simulation time was one spring–neap cycle within the respective year.

Bottom roughness is in our models described by Nikuradse´s effective roughness coefficient k_s, which relates to the bed roughness length z_0 with $z_0 \simeq k_s/30$ (Malcherek, 2010). It is composed of grain roughness, form roughness, and additional roughness. SediMorph, which is coupled with UnTRIM², calculates the grain roughness $k_{s,grain}$ at each element from the prescribed sediment distribution with $k_{s,grain} = 3d_m$, where d_m is the mean grain size. Additionally, form roughness is estimated at each time step of the simulation based on present sediments and the respective water depth and velocity, according to van Rijn (2007). Calibration factors, which determine the prevalence and importance of bedforms (ripples, mega ripples, dunes), can be specified and were varied in the calibration runs to optimise the agreement between observed and simulated water levels. As the roughness predictor underestimated roughness in the Lower Weser, we defined an additional roughness of up to 0.36 m landwards of Weser-km 55 to represent damping of the tidal wave, with some variation amongst the models. Landwards of Weser-km 55, pronounced dunes and ripples are positioned (Lange et al., 2008), which are not explicitly resolved in the models' calculation grid. Moreover, additional damping was required due to the omission of the tributaries of the Weser. Tributaries typically have low water depths and high energy dissipation rates. Thus, when tributaries are omitted, the models tend to underestimate energy dissipation, which can be outbalanced through an increase in bottom roughness.

For each model, different roughness settings were determined. Differences are caused by natural variations in sediments and bedforms between the system states, which are not represented in the models due to the lack of historical sedimentological data, and by effects induced by the different resolutions of the original topographic data. The least additional roughness was required in the model of system state 2012, where the resolution of original topographic data was comparatively high (see Table 1). The largest additional roughness in the area of Lower Weser was required in the model of system state 1981 (see Table 3). The model topography includes the deepening of the Lower Weser to SKN -9 m, which was undertaken shortly before 1981 (see Section 2.2). The deepening led to a volume increase, larger water depths, and an increase in tidal range. The model seems to overestimate this effect, possibly due to the coarse resolution and omission of tributaries, if not outbalanced by the additional roughness. The mean RMSE of tidal range in scenarios 1966, 1972, and 1981 decreased by almost 50 % after adjustment of the roughness settings by individual calibration.

Table 3. Effect of the calibration of roughness settings on results of models 1966, 1972, and 1981 compared to results of the respective models with roughness settings of 2012. Effective bed roughness was evaluated along the navigation channel (see Fig. 1).

		1966	**1972**	**1981**
Change in effective bed roughness	Along Weser-km 1.5-55.8	0.20 m (+25 %)	0.18 m (+14 %)	0.25 m (+56 %)
	Along Weser-km 55.8-126	0.015 m (+184 %)	0.019 m (+272 %)	0.010 m (+84 %)
Change in RMSE of tidal range	At stations with available measurements for all scenarios	0.17 m (-48 %)	0.19 m (-46 %)	0.19 m (-44 %)

https://doi.org/10.5194/egusphere-2022-142
Preprint. Discussion started: 28 April 2022

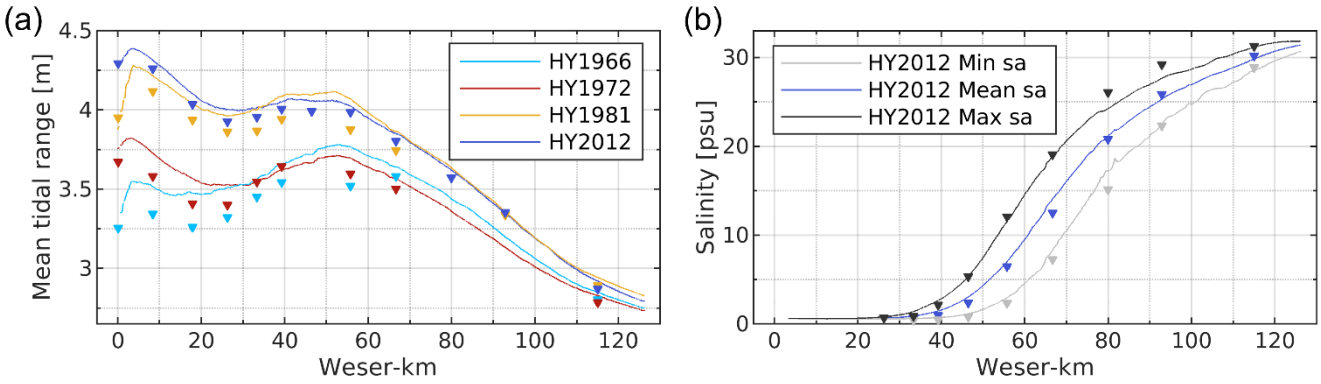

Figure 3. Mean tidal range along the navigation channel of the Weser estuary (see Fig. 1) in hindcast models of 2012, 1981, 1972, and 1966 (a) and vertically averaged mean, minimum, and maximum salinity per tide (average) in hindcast model HY2012 (b). Simulation results (lines) are compared to measured values (triangles), averaged over the same period.

The models were subsequently validated by extending the calculation time to one hydrological year (plus the preceding four weeks to allow for a model spin-up) and comparing model results to measurements. One hydrological year is defined as the time between November 1st of the previous year and October 31st of the respective year (DIN 4049-1:1992-12). The tidal range in the Lower Weser was slightly overestimated in the hindcast models (see Fig. 3a), but overall well reproduced with a mean RMSE of 0.166 m (1966), 0.114 m (1972), 0.169 m (1981), and 0.153 m (2012), averaged over stations along the navigation channel with available measurements for all scenarios. Measured values of water level and salinity only covered system state 2012. The mean RMSE in hindcast model 2012 was 0.224 m for water level, averaged over all measurement stations (see Figure 1). An overall bias of 5 cm indicated a slight, consistent overestimation of water levels. Salinity intrusion was slightly overestimated, with higher computed values than measured values in Lower Weser (see Fig. 3b). The intertidal variation in Weser-km 60–100 was slightly underestimated, with higher minimum salinity and lower maximum salinity per tide. The mean RMSE in hindcast model 2012 was 1.422 psu for mean salinity, averaged over all stations with available measured values. Overall, the magnitude and dynamics of saltwater intrusion were reproduced well in the hindcast model 2012. It is expected that the model performance will be similar for the other system states.

https://doi.org/10.5194/egusphere-2022-142
Preprint. Discussion started: 28 April 2022

4 Results

4.1 Natural variability of saltwater intrusion in the Weser estuary

As described above, salinity in the Weser estuary is subject to strong variations on different time scales (see Introduction). We studied salinity intrusion in the hydrological year 2012 based on measurement data. In each semi-diurnal tidal cycle, the 5 psu isohaline moves up- and downstream by almost 20 km (see Fig. 4a). It is located about 2 to 3 km further landward during spring tide compared to neap tide. The mean position of the 5 psu isohaline per semi-diurnal tidal cycle shifts by more than 30 km within the hydrological year 2012. A major seaward shift occurs in December and January, where the isohaline moves from Weser-km 40–73. This is induced mainly by an increase in discharge from 100 $m^3 s^{-1}$ to 1000 $m^3 s^{-1}$.

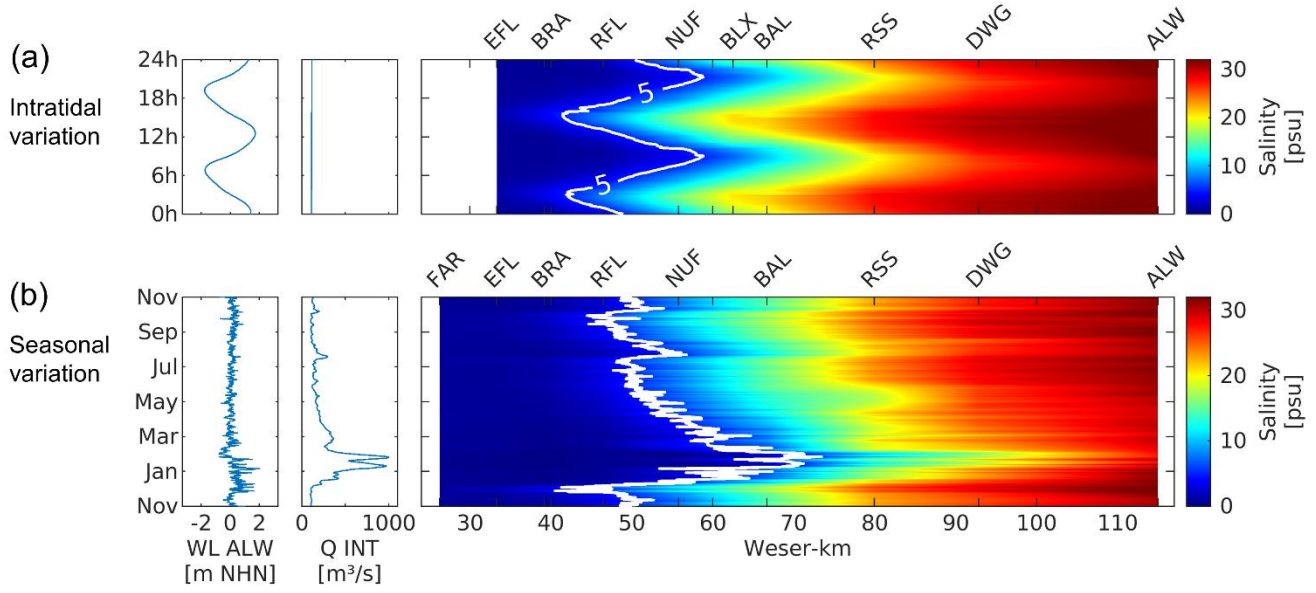

Figure 4. Intratidal and seasonal variation of saltwater intrusion in the Weser estuary. The water level at station Leuchtturm Alte Weser (ALW), discharge at station Intschede (INT), and salinity along the navigation channel of the Weser estuary are displayed on different time scales. Salinity values were interpolated linearly between measurement stations with available measurements along the navigation channel. The 5 psu isohaline is displayed in white. On top, salinity variation within one day, September 1st, 2012, is depicted (a). Below, variation within the hydrological year 2012 of the mean salinity per tidal cycle is depicted (b). We applied a moving median filter to the water level data in (b) to show the seasonal variation (filter size 12h 25min).

https://doi.org/10.5194/egusphere-2022-142
Preprint. Discussion started: 28 April 2022

4.2 Saltwater intrusion in different system states

Hydrodynamics and saltwater intrusion in the Weser estuary were simulated in hindcast models of 1966, 1972, 1981, and 2012. These models contain respective model topographies and realistic forcing (see Table 2) and they were individually calibrated (see Section 3.6). The mean tidal range in the estuary was up to 0.6 m larger in 1981 and 2012 than in 1966 and 1972 (see Fig. 3a). This reflects the impact of the deepening measures in Lower Weser in 1973–1978, which had a strong effect on tidal dynamics.

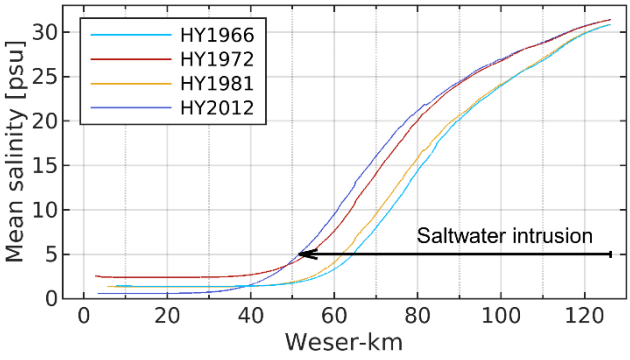

Figure 5 Annual mean, vertically averaged salinity along the navigation channel of the Weser estuary (see Fig. 1) in hindcast models of 1966, 1972, 1981, and 2012.

Saltwater intruded further in 1972 and 2012 compared to 1966 and 1981 (see Figure 5). In 1972 and 2012, the 5 psu isohaline was positioned about 10 km more landward. The reason for these large differences is particularly high discharge values in 1966 and 1981, which were on average about twice as high compared to the other system states (see Table 5). The discharge conditions fail to explain all variations. Compared to 1972, there was higher discharge in 2012; however, the position of the salinity front is about 3 km more landward. In this case, other influencing factors outweigh the impact of discharge. The mean tide level at station ALW in system state 2012 is considerably higher compared to 1972, indicating different meteorological conditions and reflecting an increase in mean sea level (Wahl et al., 2013). Moreover, the tidal range at station ALW was larger in 1981 and 2012, possibly due to topography changes (Hubert et al., 2021) and in response to the nodal tide. Along with these factors, changes in topography might affect the differences in the saltwater intrusion.

Table 4. Characteristic conditions in system states 1966, 1972, 1981, and 2012, averaged for one hydrological year based on measured values. Mean salinity and mean discharge were measured at Hemelingen (HEM) and Intschede (INT), respectively. Both stations are located upstream of the weir Bremen. Tidal mean water and tidal range in the North Sea were measured at station Leuchtturm Alte Weser (ALW).

Identifier	Mean salinity Weser (HEM)	Mean discharge Weser (INT)	Tidal mean water (ALW)	Tidal range (ALW)
HY1966	1.42 psu	508 $m^3 s^{-1}$	-0.08 m	2.80
HY1972	2.39 psu	203 $m^3 s^{-1}$	-0.16 m	2.79
HY1981	1.38 psu	477 $m^3 s^{-1}$	-0.04 m	2.89
HY2012	0.61 psu	234 $m^3 s^{-1}$	0.05 m	2.87

https://doi.org/10.5194/egusphere-2022-142
Preprint. Discussion started: 28 April 2022

4.3 Effect of discharge on saltwater intrusion in different system states

The influence of discharge on the saltwater intrusion length was analysed in each hindcast simulation. The saltwater intrusion length is here defined as the distance from the estuary mouth to the tide-averaged position of the 5 psu isohaline along the navigation channel (see Fig. 1). The estuary mouth is located at Weser-km 126.2. Amongst the simulations, discharge and other parameters differ (realistic forcing, see Table 2). Data were processed in the following way to identify correlations between discharge and saltwater intrusion length: First, the saltwater intrusion was calculated for each tidal cycle within the respective hydrological years and discharge conditions were assigned. Data points were then sorted into 50 $m^3 s^{-1}$ bins of discharge between 150–400 $m^3 s^{-1}$ and 100 $m^3 s^{-1}$ bins between 400–1100 $m^3 s^{-1}$ and averaged to reduce the effect of additional influence factors and outliers. If fewer than 10 entries were available for a category, these entries were excluded. Based on the resulting average intrusion length for the specified discharge categories, multiple nonlinear regression with interaction effects was performed with the Levenberg–Marquardt algorithm to obtain trends of the form

$$L^* = kQ^m \,, \tag{4}$$

with saltwater intrusion length L^*, factor k, discharge Q, and exponent m (see Fig. 6a). The same analysis was performed without data aggregation to examine the method's validity (see Fig. 6b). Plotted with logarithmic axes, m is the gradient of the resulting trend lines. Data from the hindcast simulation of 1972 were excluded from the analysis because the range of discharge values was insufficient for the analysis.

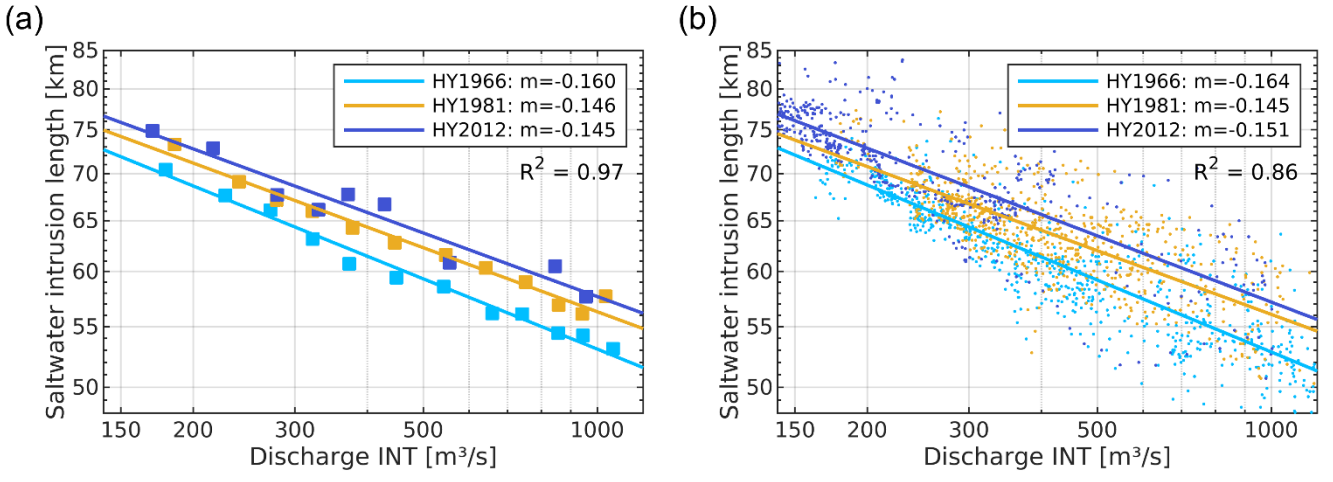

Figure 6. Saltwater intrusion length L^* (distance from the estuary mouth at Weser-km 126.2, see Fig. 1, along the navigation channel to tide-averaged 5 psu isohaline) in hindcast models of 1966, 1981, and 2012, in relation to discharge Q measured upstream of weir Bremen at station Intschede (INT). On the left, squares represent the average saltwater intrusion length for different discharge categories and lines represent trends of the form $L^*=kQ^m$ (a). The analysis was repeated with non-aggregated data points to test the method´s validity (b).

https://doi.org/10.5194/egusphere-2022-142
Preprint. Discussion started: 28 April 2022

In the scenarios representing 1966, 1981, and 2012, we identified a clear relationship between discharge and saltwater intrusion length according to Eq. (4), with $L \sim Q^{-0.15}$. As expected, the saltwater intrusion length decreases when discharge increases. This effect is greater for low discharge conditions compared to high discharge conditions. In system state 2012, the saltwater intrusion length increases by approximately 9 km if the discharge decreases from 1000 $m^3 s^{-1}$ to 380 $m^3 s^{-1}$ or from 380 $m^3 s^{-1}$ to 150 $m^3 s^{-1}$.

The trend lines for 1966, 1981, and 2012 have comparable gradients in the logarithmic plot (comparable exponents *m*). A significant difference occurs between the exponent in HY1966 compared to the exponent in HY1981 (p=0.000) and HY2012 (p=0.005) in the regression analysis with non-aggregated datapoints (Fig. 6b), pointing to a change in the system between 1966 and 1981. According to Ralston and Geyer (2019), a change in the sensitivity of saltwater intrusion to discharge could indicate a change in salt flux mechanisms. However, it has to be noted that the exact exponents depend on the definition of the saltwater intrusion length. Moreover, not only discharge, but also other influencing factors vary in the examined hindcast simulations.

Table 5. The average landward shift of depth-averaged 5 psu isohaline in the hindcast simulations, based on regression analysis (Fig. 6b).

	1966–1981	1981–2012	Overall shift 1966–2012
150 $m^3 s^{-1}$	1.7 km	2.3 km	4.0 km
300 $m^3 s^{-1}$	2.4 km	1.8 km	4.2 km
1000 $m^3 s^{-1}$	3.2 km	1.1 km	4.3 km

The trend lines are differently positioned, which indicates that with similar discharge conditions, saltwater intrusion increased between 1966 and 1981 and between 1981 and 2012. For example, with 300 $m^3 s^{-1}$ discharge, the saltwater intrusion increased by approximately 2.4 km between 1966 and 1981 and another 1.8 km between 1981 and 2012 – however, the exact shift depends on the discharge condition (see Table 6). This trend could be linked to differences in topography, i.e. the deepening measures conducted in-between the system states.

4.4 Impact of topography changes on saltwater intrusion

The effect of topography on saltwater intrusion was further examined in simulations with identical boundary values but different model topographies (scenario study). One set of simulations (1966, 1972, 1981, 2012) was conducted with the respective roughness settings, as obtained by calibration of the hindcast models. Another set of simulations was conducted with identical roughness settings (hindcast model 2012).

Simulations with different topographies and respective roughness settings confirm a notable effect of topography changes on saltwater intrusion (see Fig. 7a). The salinity front (5 psu isohaline) shifts landwards between scenario 1972 and 1981 by about 2.5 km, and between 1981 and 2012 by another 1 km. At the same time, the length of the brackish water zone (vertically averaged 5 psu isohaline to 20 psu isohaline) increases between the four scenarios from 24.2 km (1966) to 27.6 km (2012), as

https://doi.org/10.5194/egusphere-2022-142
Preprint. Discussion started: 28 April 2022

the increase in salinity along the river towards the North Sea is more gradual in scenario 2012 compared to the historical system states. The mean intratidal variation slightly decreases between 1966 and 2012.

The differences in saltwater intrusion can be linked to the topography changes between the four system states. The most significant increase in saltwater intrusion occurs between scenarios 1972 and 1981, where considerable deepening measures were conducted in the Lower Weser. An analysis of the mean depth of the navigation channel in the area where saltwater intrusion occurs (Weser-km 40–110) and the position of the vertically averaged 5 PSU isohaline in each of the scenarios suggests a strong link between mean depth and saltwater intrusion (see Fig. 7b). According to that, if the navigation channel is deepened by 1 m in Weser-km 40–110, the position of the 5 psu isohaline shifts landwards by about 2 km.

Deepening measures in the Outer Weser seem to induce an overall extension of the brackish water zone (between 5 psu and 20 psu). Between scenario 1966 and 1972 and between scenario 1981 and 2012, when deepening measures in the Outer Weser were conducted, the length of the brackish water zone increased by 1.1 km and 1.8 km. In contrast, an extension of only 0.5 km occurred between 1972 and 1981 (see Fig. 7a). An extension of the brackish water zone means that salinity increases more gradually towards the sea.

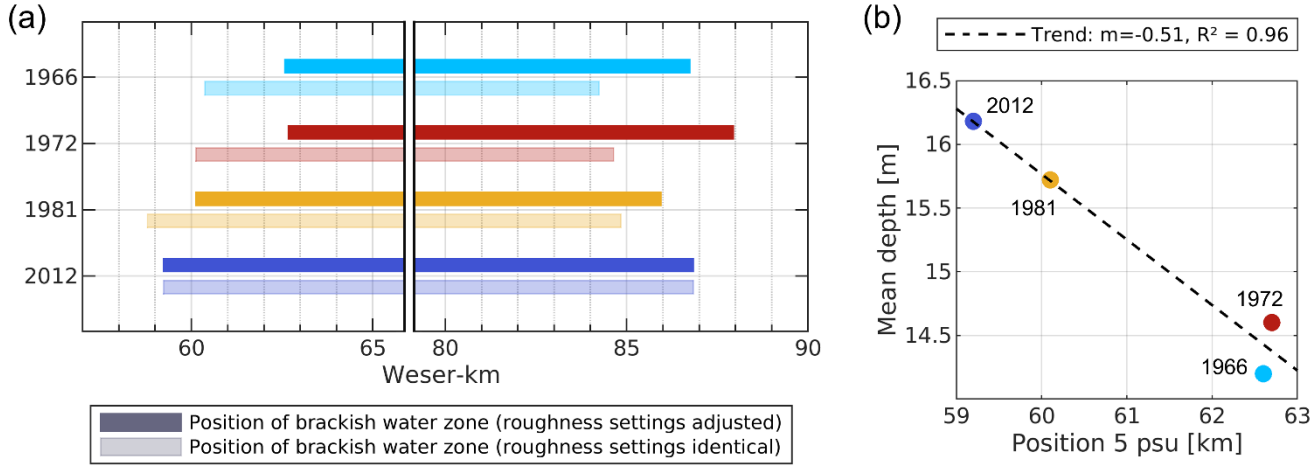

Figure 7. The left diagram (a) shows the effect of topography and roughness variation on the mean position of the brackish water zone (defined as the stretch between the vertically averaged 5 psu and 20 psu isohalines along the navigation channel, see Fig. 1). The dark colours represent simulations of the system states with adjusted roughness settings. The light colours represent simulations with identical roughness settings. On the right (b), the mean position of the vertically averaged 5 psu isohalines in simulations with adjusted roughness settings is displayed in relation to the mean depth of the navigation channel bottom between Weser-km 40 to 100 in simulations of system state 1966, 1972, 1981, and 2012 with identical boundary conditions.

4.5 Relevance of roughness calibration for the examination of saltwater intrusion in different scenarios

Calibration of the roughness settings of the different models considerably improved the model performance (see Table 3). The roughness settings balance out model effects, such as differences in the resolution of original topographic data (see Section 3.2). At the same time, they reflect roughness changes in the physical system due to natural morphological processes

https://doi.org/10.5194/egusphere-2022-142
Preprint. Discussion started: 28 April 2022

and anthropogenic interventions. Thus, the effect of topography cannot be evaluated separately from changes in bottom friction, which occur between the system states.

To evaluate the impact of the roughness calibration on the results, we conducted simulations with different model topographies but with identical roughness settings (settings of hindcast model 2012). In addition, we performed simulations with roughness settings that were obtained by calibration of the respective hindcast models. When the roughness settings are identical, the saltwater intrusion length is similar in the four scenarios. In scenario 1981, salinity values in the Lower Weser are slightly larger than in 2012; in scenario 1966 and 1972, values are slightly lower (see Fig. 7a). Because of the different resolutions of original topographic data, the bathymetry of the historical model topographies is smoother than the model topography of 2012 (see Table 1). In the simulations with identical roughness settings, it can thus be expected that there is less energy dissipation and more landward salt transport in system states 1966, 1972, and 1981 compared to 2012. This seems to counteract the expected effect of the topographical differences and approximately balance it out so that the limit of saltwater intrusion barely shifts.

Without awareness of the effects induced by the different resolutions of the original topographic data, the results could lead to the false conclusion that topography has no notable influence on the position of the salinity front. When roughness settings are adjusted according to the calibration results, effects induced by the resolution of the original topographic data are balanced out, tidal dynamics are depicted more correctly, and results suggest that there is an evident influence of topography on the position of the salinity front.

4.6 Effect of topography changes on processes governing saltwater intrusion

Saltwater intrusion in estuaries is primarily governed by the estuarine circulation, which transports salt landwards, and river flow, which transports it seawards. Channel deepening, straightening, and removal of bedforms change the estuary geometry and reduce frictional damping of the tide (Ralston and Geyer, 2019). This can affect flow volumes and velocities and, specifically, the exchange flow, tidal mixing, and the effectiveness of river discharge. The impact of topographic changes on these processes was analysed in the scenario simulations of 1966, 1972, 1981, and 2012. The scenarios contain identical boundary values but different topographies and roughness settings.

4.6.1 Exchange flow, according to the Knudsen theorem

The Knudsen theorem (Knudsen, 1900), as described in Burchard et al. (2018b), was applied to quantify exchange flow in the four scenario simulations. Transports through two cross-sections in the Lower Weser, Weser-km 55 near Nordenham and Weser-km 65 near Bremerhaven, were analysed for one spring–neap cycle. Landward and seaward volume transports (Q_{in} and Q_{out}), salt transports ($Q_{in}s_{in}$ and $Q_{out}s_{out}$), and salinity (s_{in} and s_{out}) were determined and time-averaged. Ratios and trends were similar at both cross-sections, but as expected the individual volume transports, salt transports, and salinity values were higher at Weser-km 65.

https://doi.org/10.5194/egusphere-2022-142
Preprint. Discussion started: 28 April 2022

Figure 8 displays results for Weser-km 55. Landward and seaward volume transports increase between 1972 and 1981, probably due to deepening measures in Lower Weser and the associated increase of the tidal volume. As expected, the seaward volume transport is in all scenarios higher than the landward volume transport. However, the ratio of landward to seaward volume transport slightly increases between 1972 and 1981 from 0.886 (1966 and 1972) to 0.901 (1981 and 2012). Through the increase of the landward relative to seaward volume transport and river discharge, saltwater intrudes further into the estuary. Thus, salt transport and salinity increase between 1972 and 1981. An additional increase in salt transport and salinity occurs between 1981 and 2012; this cannot be explained by the volume transports.

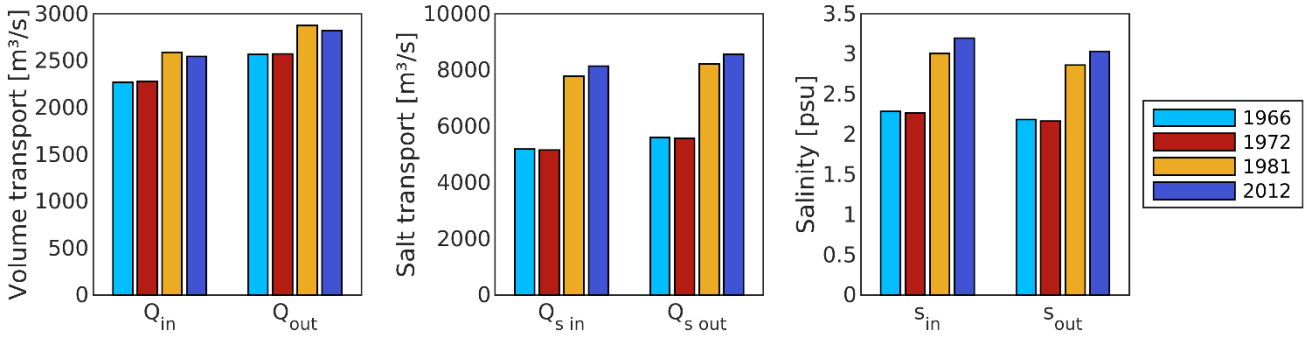

Figure 8. Landward (in) and seaward (out) volume transports (Q), salt transports (Q_s), and salinities (s) through a cross-section in Lower Weser near Nordenham, Weser-km 55, averaged over one spring–neap cycle. In all scenarios, Q_{river} is constant at 300 $m^3 s^{-1}$.

4.6.2 Residual flow and tidal mixing

As indicators for the estuarine circulation, we analysed near-bed and surface residual velocities and the potential energy anomaly (PEA) along the navigation channel of the Weser in the four scenarios and formed an average over one spring–neap cycle. The near-bed residual velocity was extracted 1.5 m above the bed. The residual velocity at the surface and near the bed diverge in approximately the same stretch along the navigation channel where the potential energy anomaly increases, indicating the estuarine gravitational circulation with the seaward residual flow at the surface and landward residual flow at the bottom (see Fig. 9). Compared to 1966 and 1972, landward residual velocities near the bed seem to be slightly stronger in 1981 and 2012 and extend further landwards. These variations indicate a slight increase in the estuarine circulation between these scenarios.

In the Weser estuary, stratification is mainly caused by salinity differences within the water column. Thus, the potential energy anomaly (PEA) is close to zero in the tidal freshwater reach and increases after Weser-km 50 (see Fig. 9b). It is largest in Weser-km 70–90, where mean salinity values of 10 psu to 20 psu occur. The spatial distribution and total values of the potential energy anomaly differ strongly between the scenarios, indicating differences in the effectiveness of tidal mixing. In Weser-km 50–70, the potential energy anomaly increases more steeply in scenario 1981 and 2012 compared to 1966 and 1972 and

https://doi.org/10.5194/egusphere-2022-142
Preprint. Discussion started: 28 April 2022

reaches higher values than in the other scenarios. Especially high peak values occur in scenario 2012, where the mean potential energy anomaly in km 70–90 is about 26 J m^{-3}.

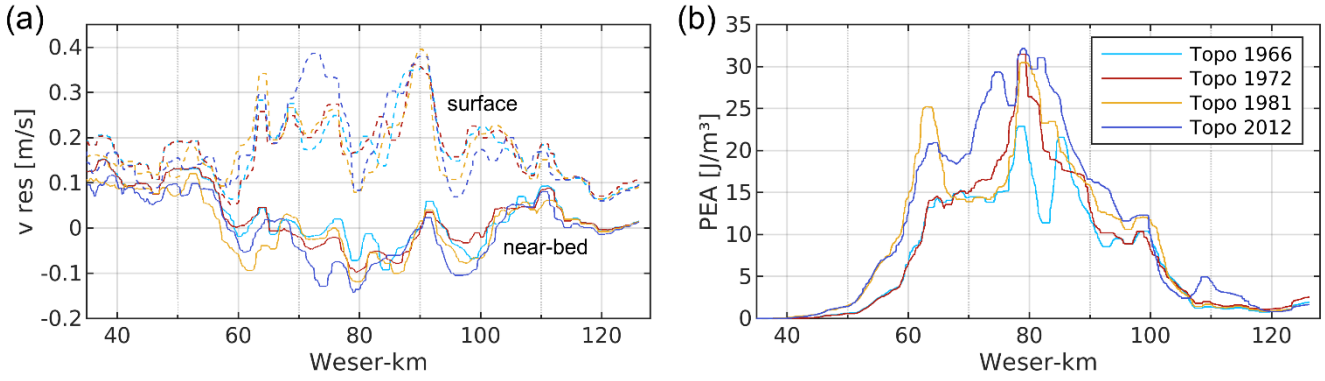

Figure 9. Residual velocity at the surface and near the bed (a) and potential energy anomaly (b) along the navigation channel of the Weser estuary in simulations of different system states with identical boundary conditions, averaged over one spring-neap cycle. We also applied a moving median filter (filter size 2 km) to minimize the importance of local effects.

4.6.3 Effectiveness of river discharge

In the scenarios study, river discharge was constant and identical. Therefore, the hindcast study simulations examined the effectiveness of river discharge to induce change to the position of the brackish water zone. According to Ralston and Geyer (2019), changes in the sensitivity of saltwater intrusion could indicate a change in salt flux mechanisms. A power-law regression analysis was conducted (see Section 4.2). We could show that no major changes in the sensitivity of saltwater intrusion to discharge occurred. There was a significant change between 1966 and 1981, which was however small. In addition to salinity, other influencing parameters differed between the simulations and lag times in the adjustment of saltwater intrusion to changed conditions were not considered in the analysis. Therefore, the small difference between 1966 and 1981 cannot be clearly attributed to a change in salt flux mechanisms.

5. Discussion

Saltwater intrusion is subject to high natural variability and salinity measurements of the past decades are not always available or exhaustive. This makes it difficult to quantify the effect of anthropogenic measures based on measurements only. With numerical simulations, we analysed the impact of anthropogenic measures on saltwater intrusion in two ways: First, we evaluated saltwater intrusion in hindcast-models of the hydrological year 1966, 1972, 1981 and 2012. We analysed the depth-averaged 5 psu isohaline as a function of discharge. Second, we evaluated the saltwater intrusion in a scenario study with identical boundary values (i.e. Q=300 $m^3 s^{-1}$).

https://doi.org/10.5194/egusphere-2022-142
Preprint. Discussion started: 28 April 2022

In the model setup, a key challenge was the lower frequency and coverage of historical measurements compared to the present state, i.e. for water level, salinity, and temperature. This can lead to differences in model accuracy and compromise the comparability of model results. In our case, a detailed validation of the historical models was not possible due to the lack of historical salinity measurements. With a systematic approach and equal treatment of the respective system states, wherever possible, we created consistency and minimized bias. For example, we generated boundary values of all models with identical methods, wherever possible, and calibrated each model individually.

It was found that an individual calibration of roughness parameters, or at least a careful evaluation of topographical data, is indispensable when setting up models with different topographies. The significance of shifts in roughness with regard to the simulation of different system states has already been highlighted by van Maren et al. (2015). However, models representing historical system states are often not calibrated (Ralston and Geyer, 2019; Grasso and Le Hir, 2019; Liu et al., 2020). We show that, without calibration and adjustment of roughness setting for individual model topographies, effects induced by the resolution of the original topographic data can strongly influence model results and lead to false conclusions. We recommend that a thorough evaluation of topographical data and, if needed, calibration of each model should always be conducted when results of models with different topographies are to be compared. An alternative approach to compensate for a low resolution of topographic data is to add artificial surface irregularities, as implemented by Hubert et al. (2021).

The analysis of hindcast results showed that, at similar discharge conditions, there is a landward shift in the position of the brackish water zone between 1966–1981 and 1981–2012. The exact distance of the shift depends on the discharge condition (see Table 6). When comparing saltwater intrusion at times with a discharge of 300 $m^3 s^{-1}$, there is a 2.4 km shift between 1966 and 1981 and a 1.8 km shift between 1981 and 2012. In the scenario study with identical boundary conditions, i.e. Q=300 $m^3 s^{-1}$, the 5 psu isohaline shifts by 2.5 km between 1972 and 1981 and by 1 km between 1981 and 2012. Both analyses show that anthropogenic measures in the Weser estuary led to an increase in the saltwater intrusion. This is in agreement with findings for other estuaries, where the navigation channel was also deepened (Andrews et al., 2017; Grasso and Le Hir, 2019; Ralston and Geyer, 2019). In the hindcast study, additional factors such as tides and salinity of the discharge and in the North Sea influence saltwater intrusion. In addition, the evaluation of saltwater intrusion depending on discharge does not account for adaptation time to changing discharge conditions. Nevertheless, results of both the hindcast study and the scenario study indicate an overall shift in the same range, 3.5–4 km. Measures in the Lower Weser, which were conducted in 1973–1978, had the highest impact. However, the exact extent of salt intrusion will also be influenced by factors not included in the model such as changes in tributaries, side channels, and the construction of waterways infrastructure.

The influence of discharge on saltwater intrusion follows the relationship $L \sim Q^{-0.15}$ in our simulations. Thus, changes in discharge have a higher impact for low discharge conditions than high discharge conditions, in agreement with previous studies (Kösters et al., 2014). Ralston and Geyer (2019) examined the relationship between discharge and saltwater intrusion length in the Hudson river in idealized scenarios with different discharge conditions. For both bathymetries, representing the present state and the predevelopment state, the sensitivity of the saltwater intrusion on discharge follows $L \sim Q^{-0.28}$. The large difference from the sensitivity found in this study (approximately $Q^{-0.15}$) may indicate limitations of the analytical approach, as the funnel-

https://doi.org/10.5194/egusphere-2022-142
Preprint. Discussion started: 28 April 2022

shaped Outer Weser estuary and the heavily engineered channel-like Lower Weser can only be very roughly approximated using analytical descriptions. In addition, different definitions of the saltwater intrusion length and different processes of estuarine mixing could contribute to the differences between the estuaries. Our analysis shows that the sensitivity of saltwater intrusion to discharge does not clearly change between the four system states. Following Ralston and Geyer (2019), this indicates that salt flux mechanisms are similar in the different system states.

The impact of anthropogenic measures on processes governing saltwater intrusion were further examined based on results of the scenario study (idealized forcing). Volume transports through cross-sections in Lower Weser increase between 1972 and 1981, indicating an increase in exchange flow. Thereby, landward transport increases more than seaward transport. We also analysed near-bed and surface residual velocities and the potential energy anomaly (PEA) on a transect along the navigation channel of the Weser. Results indicate an increase in estuarine circulation and in stratification between 1972 and 1981 in the Lower Weser due to the deepening of the Lower Weser in 1973–1978. However, fundamental changes in governing processes were not found. Possible limitations of this approach are that global trends such as a presumed increase in estuarine circulation are partially overlain with local effects. Local effects comprise e.g. an increased stratification at especially deep stretches or lower residual velocities along the navigation channel in sections where lateral flows prevail. In addition, the location of the transect is identical in all scenarios and there is deviation from the thalweg on some stretches in case of the historical system states, which could affect the results. Future studies could address these limitations by aggregating data over the entire navigation channel rather than analysing data along one transect.

6. Conclusions

Saltwater intrusion in the Weser estuary is highly variable and dependent on natural forcing factors, i.e. river discharge, as well as anthropogenic impacts, i.e. channel deepening. A systematic study of the effect of topography changes on saltwater intrusion was carried out to disentangle these overlapping influencing factors. This study used numerical models of four system states (1966, 1972, 1981, and 2012) with respective topographies to hindcast the historical development of saltwater intrusion (hindcast study) and examine the effect of anthropogenic measures (scenario study). The models were individually calibrated to compensate for different resolutions of topographic data, from which the model topographies were generated.

In the hindcast simulations, the influence of topography is overshadowed by the effect of other factors, particularly discharge. Hydrological years 1972 and 2012 are characterized by low discharge (on average about 220 $m^3 s^{-1}$), while 1966 and 1981 are high discharge years (about 490 $m^3 s^{-1}$). Thus, results of the hindcast study show a seaward shift of the mean salinity front in 1966 and 1981 by about 10 km compared with the other two system states. However, at the same discharge, a landward shift of the salinity front is indicated between 1966 and 1981 and between 1981 and 2012. This trend is confirmed in the scenario study, with identical boundary values (i.e. Q=300$m^3 s^{-1}$). Between scenario 1972 and 1981, the salinity front shifts landwards by about 2.5 km, probably due to deepening measures in the Lower Weser. A landward shift of another 1 km occurs between scenarios 1981 and 2012. It has to be noted that the exact distance by which the salinity front shifts depends on the discharge

https://doi.org/10.5194/egusphere-2022-142
Preprint. Discussion started: 28 April 2022

due to the nonlinear relation between discharge and saltwater intrusion. Analyses of the exchange flow, tidal mixing, and sensitivity to discharge indicate that the processes governing saltwater intrusion did not fundamentally change. However, the deepening measures in Lower Weser in 1973–1978 caused a small increase in estuarine circulation and stratification.

Author contribution

PK set up the numerical models and conducted simulations and analyses. AZ was involved in conceptualization, design of methodology, and interpretation of the results. PK prepared the initial draft with contributions from AZ. FK, HB and UG contributed to the discussion and revision of the paper. AZ and FK supervised the study.

Competing interests

The authors declare that they have no conflict of interest.

Acknowledgements

The work of PK, AZ and FK was funded by the Federal Waterways and Shipping Administration as part of the project "Änderungen hydrologischer Kenngrößen in der Weser seit 1970 (WeHiKo)". We thank Ulrike Schiller for her help with regard to historical topographies, Dr. Franziska Lauer for support in generation of artificial neural networks, and Dr.-Ing. Günther Lang for the development of employed postprocessing tools. The work of HB was supported by the project "Processes Impacting on Estuarine Turbidity Zones in tidal estuaries (PIETZ)", which was funded by the German Research Foundation as BU 1199/24-1.

https://doi.org/10.5194/egusphere-2022-142
Preprint. Discussion started: 28 April 2022

References

Andrews, S. W., Gross, E. S., and Hutton, P. H.: Modeling salt intrusion in the San Francisco Estuary prior to anthropogenic influence, Continental Shelf Research, 146, 58–81, https://doi.org/10.1016/j.csr.2017.07.010, 2017.

BAW: Historical digital terrain models of the Weser Estuary (HIWEST). Technical Report B3955.02.04.70168-6., Federal Waterways Engineering and Research Institute, https://hdl.handle.net/20.500.11970/107521, 2021.

BAW: Historical digital terrain model data of the Weser Estuary (HIWEST). B3955.02.04.70168-6., Federal Waterways Engineering and Research Institute, https://doi.org/10.48437/02.2020.K2.5200.0001, 2020.

BAW: Mathematical Module Sedimorph: Validation Document Version 1.1, Hamburg, 2002.

Burchard, H., Schulz, E., and Schuttelaars, H. M.: Impact of estuarine convergence on residual circulation in tidally energetic estuaries and inlets, Geophys. Res. Lett., 41, 913–919, https://doi.org/10.1002/2013GL058494, 2014.

Burchard, H. and Hofmeister, R.: A dynamic equation for the potential energy anomaly for analysing mixing and stratification in estuaries and coastal seas, Estuarine, Coastal and Shelf Science, 77, 679–687, https://doi.org/10.1016/j.ecss.2007.10.025, 2008.

Burchard, H., Schuttelaars, H. M., and Ralston, D. K.: Sediment Trapping in Estuaries, Annual review of marine science, 10, 371–395, https://doi.org/10.1146/annurev-marine-010816-060535, 2018a.

Burchard, H., Bolding, K., Feistel, R., Gräwe, U., Klingbeil, K., MacCready, P., Mohrholz, V., Umlauf, L., and van der Lee, E. M.: The Knudsen theorem and the Total Exchange Flow analysis framework applied to the Baltic Sea, Progress in Oceanography, 165, 268–286, https://doi.org/10.1016/j.pocean.2018.04.004, 2018b.

Burchard, H., Hetland, R. D., Schulz, E., and Schuttelaars, H. M.: Drivers of Residual Estuarine Circulation in Tidally Energetic Estuaries: Straight and Irrotational Channels with Parabolic Cross Section, J. Phys. Oceanogr., 41, 548–570, https://doi.org/10.1175/2010JPO4453.1, 2011.

Casulli, V.: A high-resolution wetting and drying algorithm for free-surface hydrodynamics, Int. J. Numer. Meth. Fluids, 60, 391–408, https://doi.org/10.1002/fld.1896, 2008.

Casulli, V. and Walters, R. A.: An unstructured grid, three-dimensional model based on the shallow water equations, International Journal for Numerical Methods in Fluids, 32, 331–348, 2000.

Dijkstra, Y. M., Schuttelaars, H. M., and Burchard, H.: Generation of exchange flows in estuaries by tidal and gravitational eddy viscosity-shear covariance (ESCO), J. Geophys. Res. Oceans, 122, 4217–4237, https://doi.org/10.1002/2016JC012379, 2017.

DIN 4049-1:1992-12: Hydrologie; Grundbegriffe, 2 bis 12.

Geyer, W. R. and MacCready, P.: The Estuarine Circulation, Annual Review of Fluid Mechanics, 46, 175–197, 2014.

Grabemann, I., Krause, G., and Siedler, G.: Langzeitige Änderung des Salzgehaltes in der Unterweser, Deutsche Hydrographische Zeitschrift, 36, 61–77, https://doi.org/10.1007/BF02313285, 1983.

https://doi.org/10.5194/egusphere-2022-142
Preprint. Discussion started: 28 April 2022

Grasso, F. and Le Hir, P.: Influence of morphological changes on suspended sediment dynamics in a macrotidal estuary: Diachronic analysis in the Seine Estuary (France) from 1960 to 2010, Ocean Dynamics, 69, 83–100, https://doi.org/10.1007/s10236-018-1233-x, 2019.

Hagen, R., Plüß, A., Jänicke, L., Freund, J., Jensen, J., and Kösters, F.: A Combined Modeling and Measurement Approach to Assess the Nodal Tide Modulation in the North Sea, J. Geophys. Res. Oceans, 126, 637, https://doi.org/10.1029/2020JC016364, 2021a.

Hagen, R., Plüß, A., Ihde, R., Freund, J., Dreier, N., Nehlsen, E., Schrage, N., Fröhle, P., and Kösters, F.: An Integrated Marine Data Collection for the German Bight – Part II: Tides, Salinity and Waves (1996–2015 CE), 2021b.

Hubert, K., Wurpts, A., and Berkenbrink, C.: Interaction of Estuarine Morphology and adjacent Coastal Water Tidal Dynamics (ALADYN-C), Die Küste, 89, 193–217, https://doi.org/10.18171/1.089108, 2021.

Ianniello, J. P.: Tidally Induced Residual Currents in Estuaries of Variable Breadth and Depth, J. Phys. Oceanogr., 9, 962–974, https://doi.org/10.1175/1520-0485(1979)009<0962:TIRCIE>2.0.CO;2, 1979.

Jay, D. A. and Musiak, J. D.: Particle trapping in estuarine tidal flows, J. Geophys. Res., 99, 20445, https://doi.org/10.1029/94JC00971, 1994.

Knudsen, M.: Ein hydrographischer Lehrsatz, Annalen der Hydrographie und Maritimen Meteorologie, 28, 316–320, 1900.

Kösters, F., Grabemann, I., and Schubert, R.: On SPM Dynamics in the Turbidity Maximum Zone of the Weser Estuary, Die Küste, 81, 393–408, 2014.

Krause, G.: Grundlagen zur Trendermittlung des Salzgehalts in Tide-Ästuarien, Deutsche Hydrographische Zeitschrift, 32, 233–247, https://doi.org/10.1007/BF02226051, 1979.

Lang, G.: Analyse von HN-Modell-Ergebnissen im Tidegebiet, Mitteilungsblatt der Bundesanstalt für Wasserbau, 86, 101–108, 2003.

Lange, D., Müller, H., Piechotta, F., and Schubert, R.: The Weser Estuary, Die Küste, 74, 275–287, 2008.

Liu, W.-C., Ke, M.-H., and Liu, H.-M.: Response of Salt Transport and Residence Time to Geomorphologic Changes in an Estuarine System, Water, 12, 1091, https://doi.org/10.3390/w12041091, 2020.

Malcherek, A.: Gezeiten und Wellen: Die Hydromechanik der Küstengewässer, PRAXIS, Harms, R. and Koch, S. (Eds.), Vieweg +Teubner, 2010.

Milbradt, P., Valerius, J., and Zeiler, M.: Das Funktionale Bodenmodell: Aufbereitung einer konsistenten Datenbasis für die Morphologie und Sedimentologie, Die Küste, 83, 39–63, 2015.

NLWKN: Deutsches Gewässerkundliches Jahrbuch: Weser- und Emsgebiet 2015, Hildesheim, 2018.

Ralston, D. K. and Geyer, W. R.: Response to Channel Deepening of the Salinity Intrusion, Estuarine Circulation, and Stratification in an Urbanized Estuary, J. Geophys. Res. Oceans, 124, 4784–4802, https://doi.org/10.1029/2019JC015006, 2019.

https://doi.org/10.5194/egusphere-2022-142
Preprint. Discussion started: 28 April 2022

Ralston, D. K., Talke, S., Geyer, W. R., Al-Zubaidi, H. A. M., and Sommerfield, C. K.: Bigger Tides, Less Flooding: Effects of Dredging on Barotropic Dynamics in a Highly Modified Estuary, J. Geophys. Res. Oceans, 124, 196–211, https://doi.org/10.1029/2018JC014313, 2019.

Rasquin, C., Seiffert, R., Wachler, B., and Winkel, N.: The significance of coastal bathymetry representation for modelling the tidal response to mean sea level rise in the German Bight, Ocean Sci., 16, 31–44, https://doi.org/10.5194/os-16-31-2020, 2020.

Simpson, J. H.: The shelf-sea fronts: Implications of their existence and behaviour, Phil. Trans. R. Soc. Lond. A, 302, 531–546, https://doi.org/10.1098/rsta.1981.0181, 1981.

Simpson, J. H., Brown, J., Matthews, J., and Allen, G.: Tidal Straining, Density Currents, and Stirring in the Control of Estuarine Stratification, Estuaries, 13, 125, https://doi.org/10.2307/1351581, 1990.

van Maren, D. S., Winterwerp, J. C., and Vroom, J.: Fine sediment transport into the hyper-turbid lower Ems River: The role of channel deepening and sediment-induced drag reduction, Ocean Dynamics, 65, 589–605, https://doi.org/10.1007/s10236-015-0821-2, 2015.

van Rijn, L. C.: Unified View of Sediment Transport by Currents and Waves: I Initiation of Motion, Bed Roughness, and Bed-Load Transport, Journal of Hydraulic Engineering, 133, 649–667, https://doi.org/10.1061/(ASCE)0733-9429(2007)133:6(649), 2007.

Wahl, T., Haigh, I. D., Woodworth, P. L., Albrecht, F., Dillingh, D., Jensen, J., Nicholls, R. J., Weisse, R., and Wöppelmann, G.: Observed mean sea level changes around the North Sea coastline from 1800 to present, Earth-Science Reviews, 124, 51–67, https://doi.org/10.1016/j.earscirev.2013.05.003, 2013.

Wetzel, V.: Der Ausbau des Weserfahrwassers von 1921 bis heute, in: Jahrbuch der Hafenbautechnischen Gesellschaft, edited by: Schwab, R. and Becker, W., Springer Berlin Heidelberg, 1029–1136, 1988.

Wiltshire, K. H., Malzahn, A. M., Wirtz, K., Greve, W., Janisch, S., Mangelsdorf, P., Manly, B. F. J., and Boersma, M.: Resilience of North Sea phytoplankton spring bloom dynamics: An analysis of long-term data at Helgoland Roads, Limnology and Oceanography, 53, 1294–1302, https://doi.org/10.4319/lo.2008.53.4.1294, 2008.

Winterwerp, J. C., Wang, Z. B., Braeckel, A., Holland, G., and Kösters, F.: Man-induced regime shifts in small estuaries - II: a comparison of rivers, Ocean Dynamics, 63, 1293–1306, 2013.